Received: 02 March 2023 | Revised: 09 April 2023 | Accepted: 16 April 2023
DOI: 10.22034/ecc.2023.391617.1616
Eurasian Chemical Communications
SAMI

FULL PAPER

High photocatalytic performance of ZnO and ZnO/CdS nanostructures against reactive blue 4 dye

Suaad Abd M.A. Noor*|Amer M.J. Al-Shamari

Department of Pharmacy, College of Science, University of Kufa, Kufa, Iraq

Heterogeneous photocatalysis is an effective wastewater treatment technology for the removal of tissue effluents and some contaminants. Among the effective catalytic treatments, hybrid semiconductor photocatalysts have been widely applied and have received more attention in the past few decades where particles and nanocomposites (ZnO and ZnO/CdS) were prepared by hydrothermal method from raw materials, and its photocatalytic activity was studied using reactive Blue 4 dye under the influence of ultraviolet radiation. The prepared nanocomposites are characterized using various physicochemical techniques including X-ray diffraction (XRD), Field emission scanning electron microscopy (FE-SEM), and Transmission electron microscopes (TEM) analyses. Their photodegradation results revealed that ZnO doped ZnO/CdS nanocomposites show impressive activity towards photodegradation of (Reactive Blue 4) dye. The prepared kinetic diagrams showed a pseudo-first-order interaction. The results of the dissociation efficiency of the dye solution (Reactive Blue 4) dye with the ZnO surface were greater than the surface of ZnO/CdS nanocomposite, and the rate constant was calculated for each of them.

***Corresponding Author:**
Suaad Abd M.A. Noor
E-mail: suaad.toobi@uokufa.edu.iq
Tel.:+9647809665323

KEYWORDS

Photocatalysis properties; chemical synthesis; ZnO; ZnO/CdS; semiconductors.

Introduction

Due to the rapidly expanding population and the increasing incidence of contaminants, there is an urgent demand for clean water resources as one of the prerequisites of our everyday lives [1]. Massive amounts of synthetic dyes, which are chemically and physically stable chemicals and unsafe for the environment, are utilized in the textile industry. Since it is stable and soluble in water, synthetic colors accumulate in wastewater and industrial effluent [2-4].

Reactive Blue 4 (RB 4) is one of the hazardous substances in water. RB 4 is an anionic dye used in a variety of industries, including the textile and wood industries. The RB4 degradation in water is a significant problem in the industry since the inability to remove it has put the environment and living things in danger. Several methods for removing RB 4 from aqueous environments, including adsorption [5] biosorption mechanism, membrane, and photocatalytic process have recently been discovered. The majority of conventional methods for RB 4

removal have drawbacks since they produce secondary pollutants including adsorption and they are either expensive, like the membrane method, or use a biosorption mechanism [6]. Yet, due to its distinct advantages without manufacturing secondary pollutants, the photocatalytic approach for the breakdown of dangerous substances becomes relevant [7].

The photocatalyst converts the toxic chemical into beneficial byproducts like water and carbon dioxide [8]. It is simple to use the photocatalyst repeatedly, especially when it possesses magnetic qualities. Physical, chemical, and biological approaches to conventional water treatment have been developed to manage textile wastewater [9]. However, due to dyes' highly water-soluble and bio-persistent nature, these approaches are damaging and ineffectual in their total destruction [10]. To decompose the organic pollutants and save the environment from their harmful consequences, a treatment technique that is environmentally benign, clean, effective, and cost-effective is urgently needed [11]. A possible method for treating sewage is photocatalysis. The photocatalytic oxidation approach, which is recognized as a safe and efficient method for treating wastewater, can convert organic pollutants adsorbed on the catalyst surface into benign carbon dioxide, water, and inorganic salts without causing secondary contamination [12].

ZnO is one of the extensively researched semiconductor photocatalysts due to its low cost, nontoxic makeup, high quantum efficiency, and environmental friendliness [13-15]. A possible method for treating sewage is photocatalysis. The photocatalytic oxidation approach, which is recognized as a safe and efficient method for treating wastewater, can convert organic pollutants adsorbed on the catalyst surface into benign carbon dioxide, water, and inorganic salts without causing secondary contamination [12]. ZnO/CdS nanocomposites [16] have been used for photocatalytic applications because they improve UV light absorption and offer efficient charge transport. The highest amount of charge carriers resides at the surface of nanocatalysts due to these morphologies' dimensional anisotropy, which also causes a flow of charge along the nanocatalyst surface. High photoactivity is further made possible by its facilitation of high charge separation and minimal recombination [17]. With a band gap of 2.4 eV and a strong optical absorption coefficient, CdS is a transition metal sulfide [18]. According to numerous reports, the formation of binary composites, such as ZnO-CdS, is to blame for the increase in photocatalytic activity in the visible range [19]. Nanocomposites have a number of advantages, including high charge separation, a substrate for heterogeneous nucleation, high charge carrier mobility, and an extended charge carrier life [20].

In this study, preparation of ZnO and ZnO/CdS nanocomposite, characterization methods, and the experimental setup for performing a thorough photocatalytic degradation process are all covered in this article, and they used to photocatalytic effect on RB 4 dye.

Experimental

Materials and methods

Reactive Blue 4 (RB4) (Santa Cruz Biotechnology 95%) was used for photocatalytic degradation studies. The chemical structure of RB4 is given in Scheme 1. Materials Zinc Nitrate $Zn(NO_3)_2.6H_2O$ and sodium hydroxide (NaOH) pellets from Sigma-Aldrich. All chemicals used were analytical grade without further purification. Distilled water was used throughout the experiment. Cadmium nitrate tetrahydrate $[Cd(NO_3)_2.4H_2O]$, thiourea (CH_4N_2S), and hexamethylenetetramine $[(CH_2)_6N_4$, HMT] and polyvinyl pyrrolidone (PVP) was purchased from Sigma Aldrich.

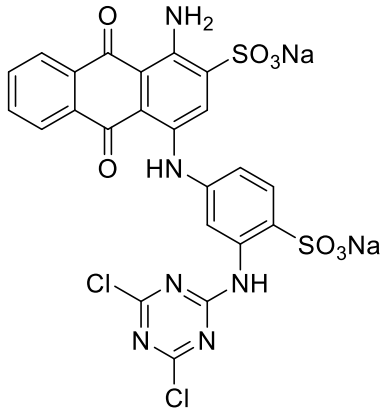

SCHEME 1 Chemical structure of RB4

Synthesis ZnO of nanoparticles using the hydrothermal method

The hydrothermal process is used to create the zinc oxide nanoparticles. Sodium hydroxide (NaOH) pellets and zinc nitrate [$Zn(NO_3)_2.6H_2O$] pellets are used. Deionized water (DIW) was utilized throughout the experiment to dilute all the chemicals needed to create zinc oxide nanoparticles. The nanoparticles were created using the hydrothermal technique. In 30 mL of deionized water, 0.5 M zinc nitrate solutions were made and agitated for 30 minutes. 5 M NaOH solution in the meantime was made by swirling 30 mL of deionized water for the same amount of time that weighted NaOH grains were mixed. The prior solution is gradually supplemented with it while being constantly stirred, up until the reactants' pH reaches 12 [21-26]. This solution mixture was put into a 70 mL Teflon-lined stainless-steel autoclave and under 100°C for 2 hours. After that, the autoclave was removed and left to gradually cool to ambient temperature. The finished product was then dried and put together after being washed repeatedly with deionized water.

Synthesis ZnO@CdS of nanocomposite using the hydrothermal method

To create the ZnO/CdS nanocomposite, 0.0538 g of ZnO nanoparticles were added to a mixture of 0.0388 g Cd(NO), 3.99 g PVP, and 0.0150 g $SC(NH_2)_2$. After thoroughly combining all ingredients, the mixture was immediately transported to an autoclave made of stainless steel that was lined with teflon (100 mL). The hydrothermal synthesis was performed at 120°C for 2 hours. After the installation period is through, the product is separated using a centrifuge, cooled at room temperature, washed with distilled water, and dried in an oven at 70°C [27].

Results and discussion

XRD analysis

The Figure 1 depicts the XRD pattern for ZnO NPs. The chemical contains nanoparticles up to big and identifiable spectrum peaks. The study of the XRD result determined the density and complete breadth at half the maximum size and position. Peaks were seen in nine diffractions, at 2, 31.67, 34.34, 36.20, 47.46, 56.54, 62.83, and 67.91°, respectively, corresponding to the crystal levels of (100), (002), (101), (102), (110), (103), and (112). At (101) peaks, broad neutrality and a sharper peak were seen without the peak twisting. These numerous peaks revealed crystals oriented randomly. The Debye-Scherer formula produced ZnO NPs with an average crystal volume of (D) indicated the ZnO powder with hexagonal nanostructures [28]. The ZnO nanoparticles' acquired XRD result is in good agreement with prior literature reports. The data XRD breakdown shows that the ZnO NPs sample has a high degree of crystalline quality due to its narrow and strong diffraction peaks, particularly in (100), (002), and (101).

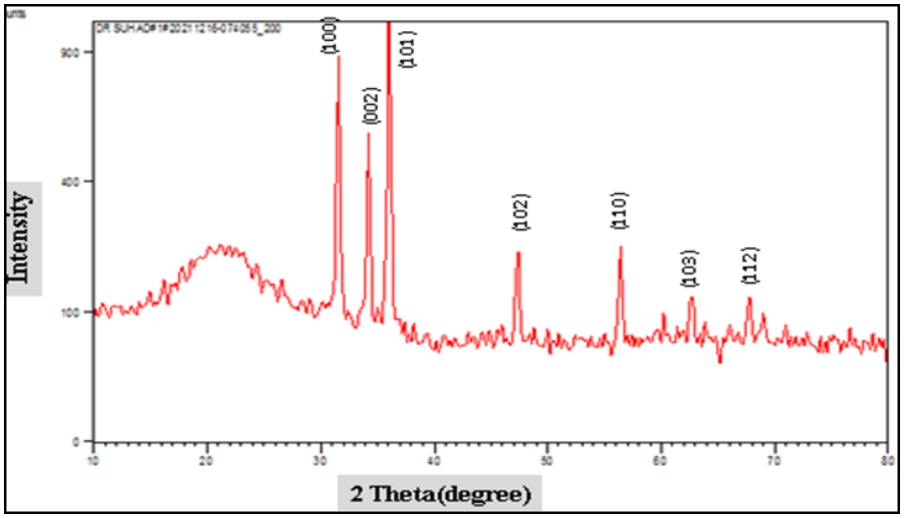

FIGURE 1 XRD pattern of ZnO nanostructures

The ZnO/CdS nanocomposite's crystalline structure was ascertained using X-ray diffraction investigation, as shown in Figure 2. The XRD pattern of pure ZnO exhibits reflections in accordance with the material's well-known hexagonal symmetry (JCPDS: 36-1451) [29]. According to XRD analysis of ZnO@CdS, the diffraction peaks of CdS can be attributed to a mixture of cubic (JCPDS: 10-0454) and hexagonal (JCPDS: 41-1049) phases. Peaks for both of the components (ZnO and CdS) can be seen in the ZnO-CdS complex, clearly demonstrating the complex's creation. There are diffraction peaks in the ZnO-CdS composite nanostructures centered at ZnO hexagonal phase may be found at 31.9, 34.7, 36.5, 48.4, and 57.1°, while CdS can be found at 25.3, 26.8, 28.6, 44.4, and 52.8°, corresponding to the (100), (002), (101), (102), and (110) crystal planes. It should be noted that only the hexagonal phase of CdS can be accurately mapped to the CdS peaks in the composite. In particular, the presence of three peaks in the composite between 25 and 30°, which correspond to the (100), (002), and (101) levels of hexagonal symmetry, rather than the single peak in CdS at 26.8°, which corresponds to the (111) level cubic symmetry, shows that hexagonal symmetry makes up the majority of CdS presence in the composite. This can be as a result of aided growth.

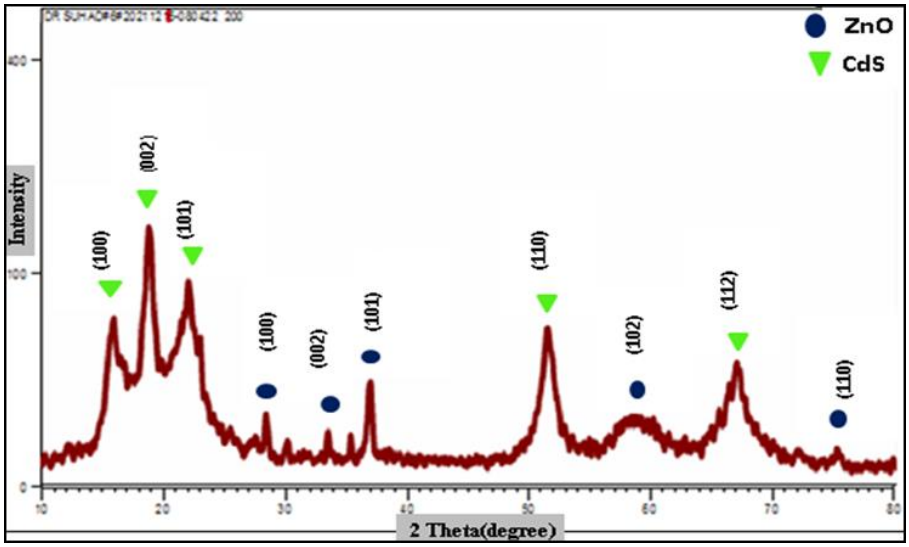

FIGURE 2 XRD pattern of ZnO/CdS nanocomposite

FE-SEM images of ZnO nanoparticles are depicted in Figure 3. It has been observed that the average diameter of ZnO was obtained 23.63 nm.

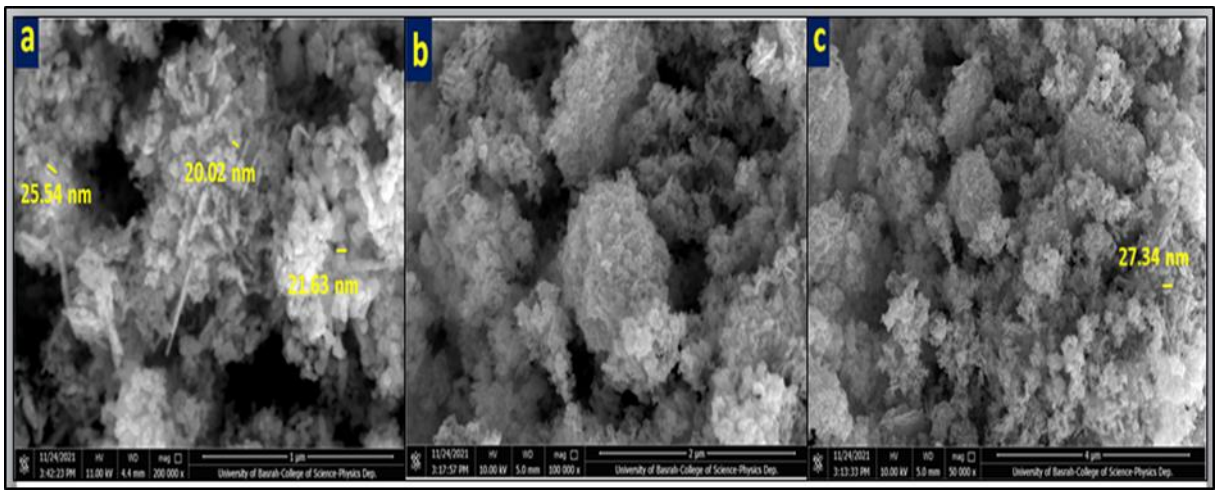

FIGURE 3 Images FE-SEM of ZnO nanoparticles

Figure 4 displays FE-SEM pictures of the ZnO@CdS nanocomposite's structural details.

The size of the nanoparticles ranges almost entirely between 10-71.5 nm and has an average diameter of 45.49 nm. Likewise, the images display the size, form, and manner of gathering spherical nanoparticles.

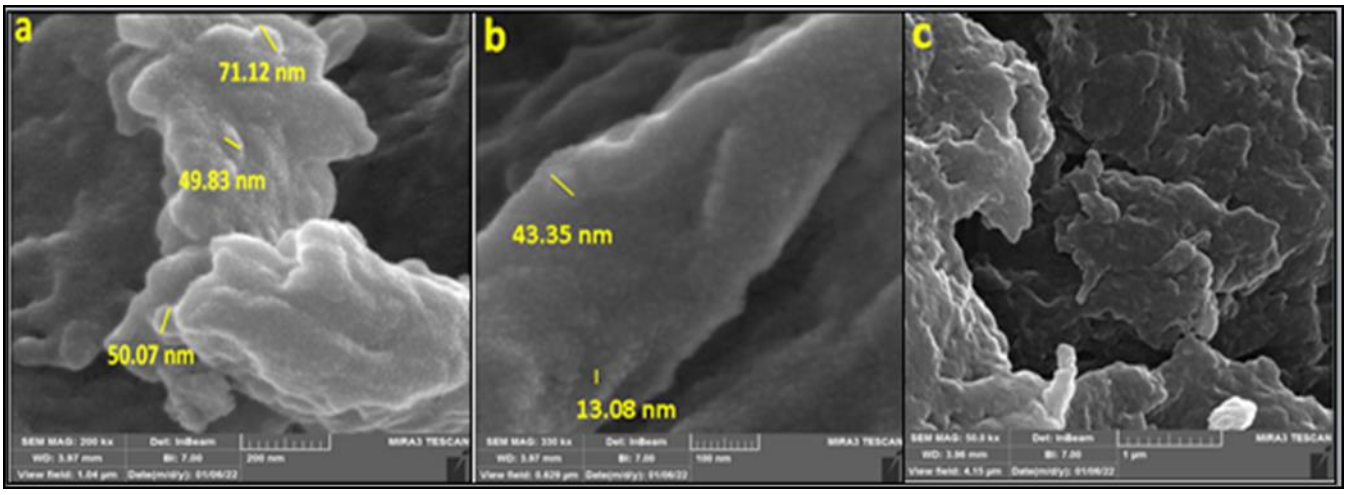

FIGURE 4 Shows images FE-SEM of ZnO@CdS nanocomposite

TEM technology was used to examine produced nanoparticles and nanocomposite materials. ZnO, and ZnO@CdS formations as seen in TEM pictures. ZnO nanoparticles have a spherical form and range in size from 17.99 to 77.40 nm, as illustrated in Figure 5. The ZnO@CdS nanocomposite's nanoparticles are shown in Figures 6 and 7 in terms of their size and form 13-71.12 nm.

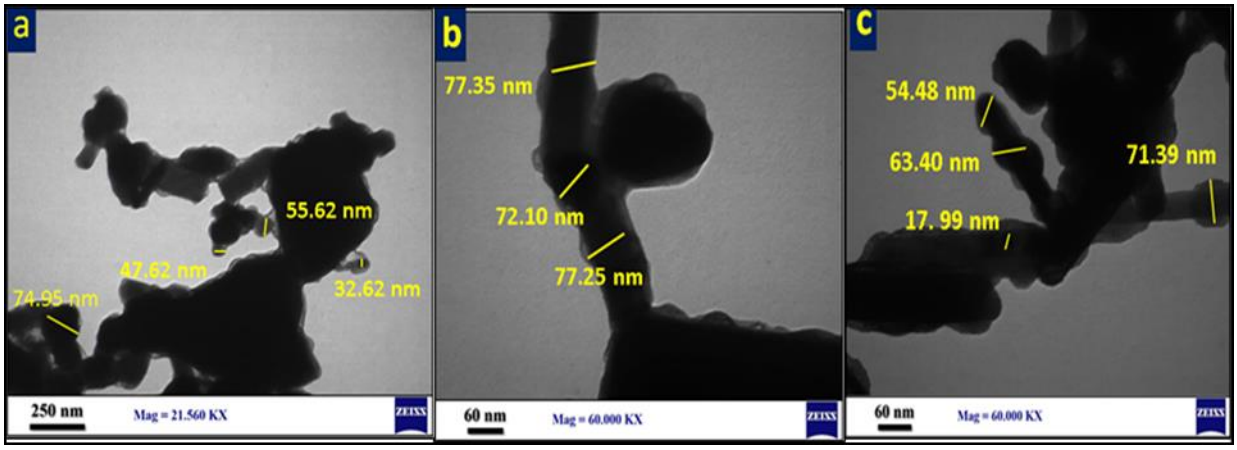

FIGURE 5 Images TEM of ZnO nanoparticle

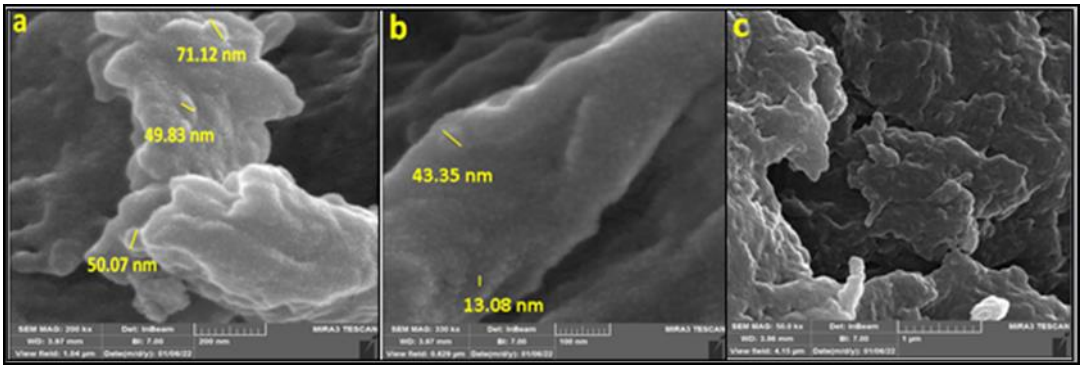

FIGURE 6 Images TEM of ZnO@CdS nanocomposite

Images TEM of ZnO@CdS nanocomposite

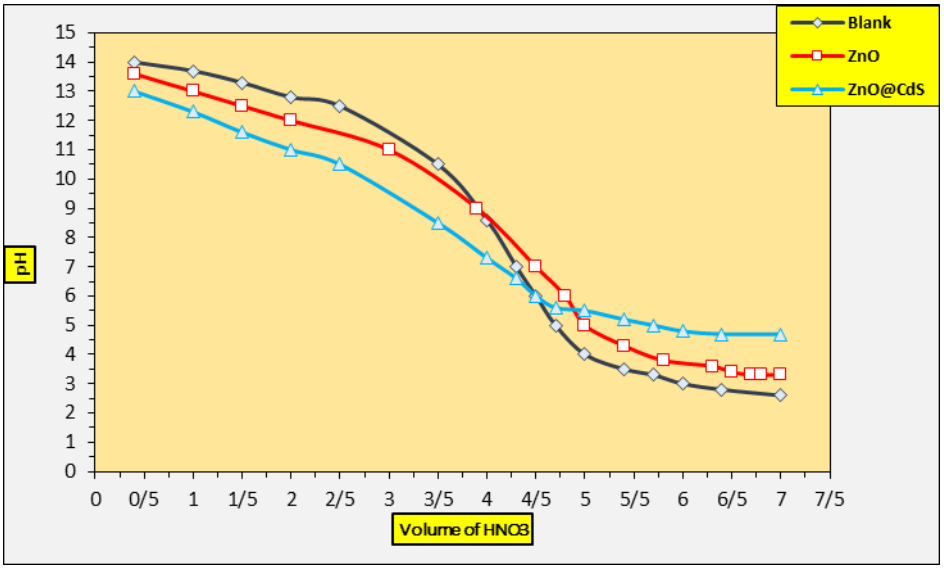

FIGURE 7 Determination of the point zero charge by potentiometric mass titration technique to ZnO NPs, and nanocomposite ZnO@CdS

The presence and absence of the nanomaterial surface and the nanocomposite surface as a catalyst, in which the dye dissociation speed was tested in three stages,

are factors affecting the photodegradation of RB4 dye and the conditions affecting the photodegradation speed. The initial stage in the dark box was the presence of RB4 dye as well as the catalyst only after determination and calculation of the best surface weight, best dye concentration, and the best pH medium. The second phase. In the third step, the dissociation rate and preferred method are studied with respect to the catalyst surface and the UV light. The surface of nanomaterials and nanocomposites (ZnO and ZnO/CdS) generated for the investigation were compared with dye dissociation, and the effect of temperature on how quickly the RB4 dye separated from the nanocatalyst surface. For materials and nanocomposites prepared with the dye according to the different reaction conditions that were mentioned, as their values were calculated after adjusting the reaction conditions, the standard curves depicting the dissociation of the dye were drawn in the three stages that were mentioned, where the drawing was between the value of C/C_0, and the time once, between $\ln C/C_0$, and again. Figures 8 and 9 depict the dye dissociation reaction for the two surfaces, while the catalyst is present but without radiation. Due to the adsorption of RB 4 dye on the surfaces of the catalyst nanomaterials, the ZnO surface exhibits the greatest reduction in the C/C_0 value when compared to the binary surface ZnO/CdS, which is dependent on the catalyst nanomaterial's surface area. The kind of catalyst also plays a part in how the concentration of the RB 4 dye solution changes over time when ultraviolet light radiation is present. In addition, each of the produced catalysts has an energy band gap, which is highest for the ZnO catalyst surface from the ZnO/CdS binary surface.

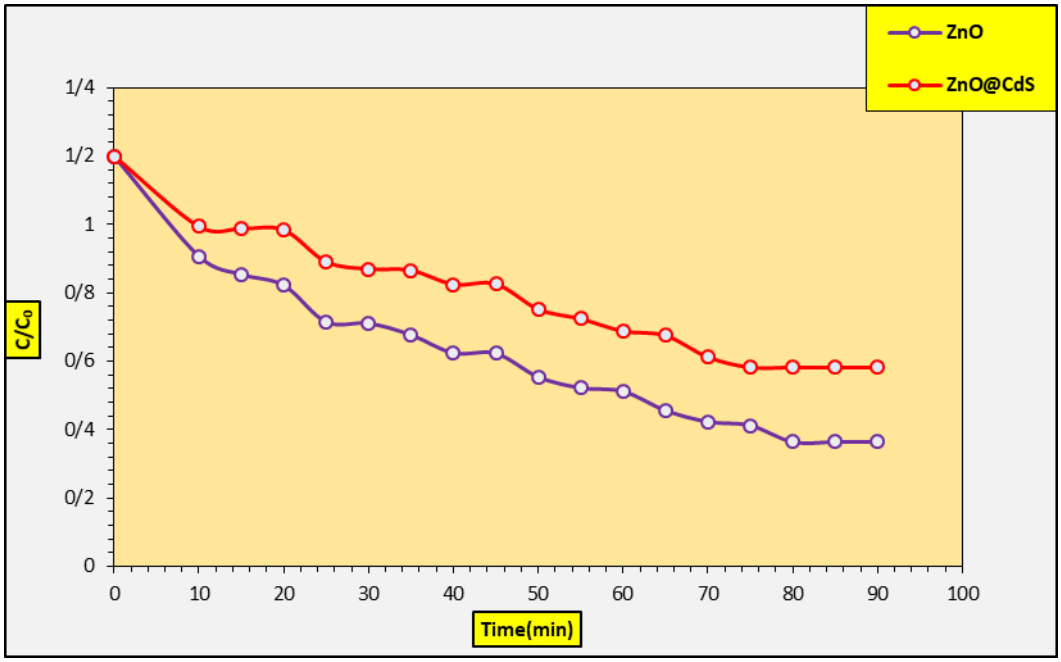

FIGURE 8 The C/C_0 vs. time for RB 4 in the dark for prepared surfaces nanomaterials and nanocomposites

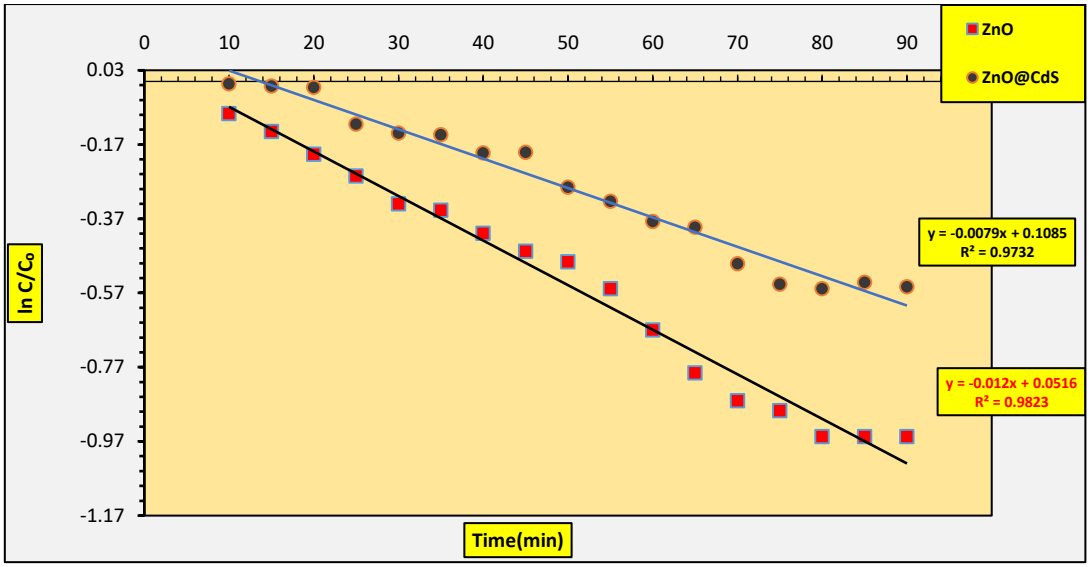

FIGURE 9 The ln C/C_0 vs. time for RB 4 dye in the dark for prepared surfaces nanomaterials and nanocomposites

In the second stage of the dye's photodegradation reaction, shown in Figure 10, the dye solution was employed at two concentrations (10 ppm and 15 ppm) with UV light irradiation, but without the usage of the nanocatalyst surface (the catalyst), which indicates a minor drop in the dye's C/C_0 value.

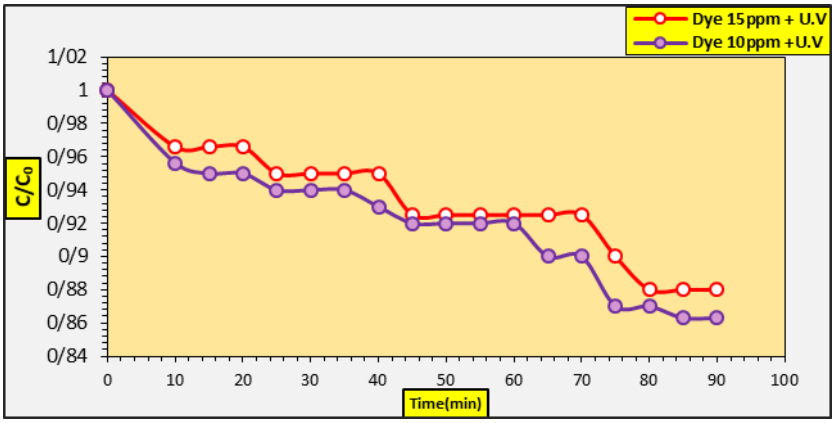

FIGURE 10 C / C_0 versus time for RB 4 dye in the presence of UV light only

Figure 11 illustrates the dye dissolution in the presence of a nanocatalyst surface and an ultraviolet (UV) radiation source during the third stage. Although the two figures depict a comparison of the two surfaces and their choice, as determined by the gradation below: ZnO >ZnO@CdS. In terms of the rate and volume of RB4 dye dissociation, the single nano-surface performs better than the bilateral. When comparing the stages of the reactions in the dark and under the influence of ultraviolet light, which were illustrated in the previous figures, where the change was in the dye's concentration, the photolysis of the RB4 dye with the individual metal oxides ZnO with the binary and nanocomposites ZnO@CdS, respectively, But, in the dark, it is also low because of the dye's adsorption on the surface of the catalysts, which depends on surface area, along with a drop in concentration of the dye in the presence of the surface. While the dye concentration

decreases when the surface is present and ultraviolet radiation is present, it is also lower in the dark due to the dye's adsorption on the surface is absent, the effect is quite small, but when UV catalysts, which are surface area-dependent. When ultraviolet radiation and the catalyst surface are combined, the dye dissolves with a high degree of efficiency on the surfaces of the catalysts. Efficiency is dependent on the catalyst surface areas and the rate at which the dye dissociates on those surfaces.

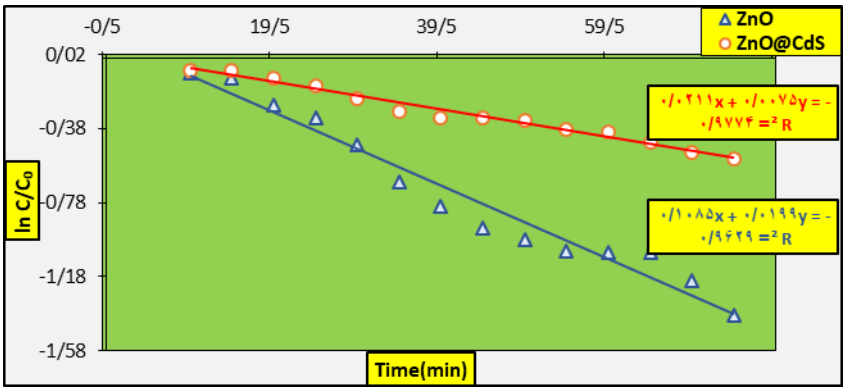

FIGURE 11 $\ln C/C_0$ versus time for dyeing RB 4 in the presence of nanomaterials and catalyst nanocomposites prepared in the presence of UV radiation

Effect of different parameters on photocatalytic degradation of RB 4 Solution

Effect of RB 4 dye concentration

The impact of adjusting the RB 4 dye solution's concentration on the effectiveness of photocatalytic degradation to extract the best concentration of the dye to use later to extract the best weight for the nanocatalyst surface, the process under the influence of ultraviolet radiation was tested using a constant weight of the manufactured nano-surface (ZnO and ZnO/CdS) (0.1 g). The impact of each dye solution concentration and the catalyst nanosurface weight on the dye solution's photocatalytic degradation efficiency with a ZnO surface under constant temperature and surface weight conditions with varying dye solution concentrations, where concentrations ranged from 5-25 ppm. We see that the dye solution's best (87%) at a concentration of 15 ppm. On the photocatalytic degradation efficiency of the dye solution, each dye solution concentration and the weight of the catalyst nanosurface are important factors. Table 1 displays the P.D.E. of the dye solution with a ZnO surface under constant temperature and surface weight conditions with shifting dye solution concentrations, where concentrations ranged from 5-25 ppm. The best P.D.E. dye solution with a concentration of 87% is noted 15 ppm. Table 1 displays the P.D.E. values for each dye concentration together with its corresponding rate constant values. With regard to the dye concentrations utilized in terms of their dissociation rates with the catalyst nanosurface effective, we observe from the obtained results that the value of the rate constant K (0.0781 min^{-1}) is larger at a concentration of 15 ppm.

TABLE 1 The (P.D.E.%) and rate constant of RB4 under influence of ultraviolet radiation (U.V) for ZnO NPs at laboratory temperature

Conc. RB4 dye solution ppm	P.D.E.%														K (min)$^{-1}$
	10 min	15 min	20 min	25 min	30 min	35 min	40 min	45 min	50 min	55 min	60 min	65 Min	70 min	75 min	
5	6.67	7.14	21.43	24	25.71	33.12	38.57	40.32	50.3	61.43	66.45	68.77	70	75.75	0.0196
10	6.52	19.57	23.91	26.1	28.26	36.96	41.3	43.48	52.17	63.04	69.6	78.26	78.26	78.26	0.0219
15	7.46	22.39	37.31	41.79	46.27	53.73	61.19	67.16	71.64	74.63	83.58	86.56	86.66	87	0.0339
20	5.28	8.28	20.73	23.96	22.03	28.54	33.76	38.92	45.98	56.98	57	57.21	58.06	58.08	0.0141
25	5	7.22	15.70	19.84	21.79	27.27	28	29.78	34.71	45.46	46.45	48	52.06	52.1	0.0109

As for the surface of the ZnO/CdS nanocomposite with the dye solution, the best concentration was (10 ppm). As it can be seen in Table 2, the dye solution has high photocatalytic degradation efficiency (42.68%) at a concentration of 10 ppm and that the rate constant K is also higher at this concentration (0.0958 min^{-1}) than it is at the other concentrations.

TABLE 2 The (P.D.E.%) and rate constant of RB 4 under influence of ultraviolet radiation (U.V) for ZnO/CdS nanocomposite at laboratory temperature

Conc. RB4 dye solution ppm	P.D.E.%														K (min)$^{-1}$
	10 min	15 min	20 min	25 min	30 min	35 min	40 min	45 min	50 min	55 min	60 min	65 min	70 min	75 min	
5	3.03	9.091	9.091	12.12	15.15	15.15	18.18	21.2	24.24	30.3	36.36	39.39	39.39	39.4	0.0075
10	3.64	9.75	9.88	12.54	15.65	16.12	18.68	21.87	25.65	31.74	38.55	41.57	42.67	42.68	0.0416
15	2.54	8.76	8.912	10.23	12.22	13.54	16.66	18.34	20.34	25.54	27.54	32.38	33.54	33.55	0.0066
20	2.32	8.32	8.512	9.76	10.22	12.35	13.43	16.61	18.32	20.32	24.54	24.88	25.43	25.45	0.0037
25	2	7.23	8	9.13	9.77	10.23	11.12	12.32	16.02	18.13	21.43	21.52	21.74	21.75	0.0034

Effect of catalyst weight

The decomposition rate was examined using various catalyst weights in the range of (0.05-0.15 g) under the influence of ultraviolet radiation. The catalyst surface works to reduce the activation energy, and thereby it is possible to obtain more molecules with activation energy, and then the reaction rate increases. Little quantities are used when catalysts are utilized. After a certain point, increasing the catalyst quantities utilized in the reaction does not result in an increase in reaction rates [30]. Table 3 displays the effectiveness of the RB4 dye's photocatalytic degradation after extracting it at its highest concentration (15 ppm) using surface ZnO NPs of various weights while subjected to UV radiation for 85 minutes. When weighing (0.075 g), the highest value of photocatalytic degradation efficiency (82.33%), and the rate constant k (0.05942 min^{-1}). The lowest value of k is (0.0272 min^{-1}), obtained when utilizing the surface weight, while the lowest value of photocatalytic degradation efficiency (55.1%) was achieved when weighing (0.15 g). The rise in the weight of the catalyst surface caused an increase in the active sites on the catalyst surface, which is what caused the values of P.D.E and k to increase and decrease. A higher than necessary concentration of the catalyst will result in more suspended particles in the dye solution, which will subsequently turbidize the suspension and reduce penetration. Radiation, followed by light scattering and reduced light penetrating the remedy [31,32]. Moreover, utilizing more catalyst surfaces

reduces the activation of the activated molecules by causing them to collide with the ground state molecules, which dominates the process and slows down the rate of the reaction [33]. For the produced catalyst nanosurface exposed to the UV light, Table 3 displays the P.D.E. values and the K values of the ZnO surface with the RB 4 dye solution at various weights.

TABLE 3 The (P.D.E.%) and rate constant of RB4 under UV irradiation vs. catalyst weight of ZnO NPs at laboratory temperature

Catalyst weight (g)	P.D.E. %																K $(min)^{-1}$
	10 min	15 min	20 min	25 min	30 min	35 min	40 min	45 min	50 min	55 min	60 min	65 min	70 min	75 min	80 min	85 min	
0.05	22.07	25.97	31.17	35.07	38.96	41.56	46.75	47.06	57.14	64.94	64.94	67.53	72.73	72.73	73.77	74	0.0208
0.075	12.5	18.75	31.25	37.5	44.5	51.56	59.38	62.5	65.63	70.31	73.44	78.13	78.4	79.69	82.25	82.33	0.0258
0.1	7.46	17.91	25.37	41.79	46.29	47.29	52.24	55.7	56.7	57.71	59.7	61.19	65.67	70.15	70.43	71.12	0.0222
0.125	4.11	12.33	17.81	26.03	38.36	41.09	45.21	47.95	49.32	52.05	56.16	58.9	58.9	61.64	61.66	61.66	0.0141
0.15	6.41	10.26	12.82	21.49	30.33	35.89	36.74	38.03	43.72	45.28	51.13	51.7	52.54	53.10	54.1	55.1	0.0118

The P.D.E. values and rate constant K values of the ZnO/CdS nanocomposite under the influence of UV irradiation are shown in Table 4. After extracting the most amount of RB 4 dye possible from the ZnO/CdS nanocomposite's surface at 10 ppm. Where the rate constant K (0.0253 min^{-1}) and the maximal value of P.D.E. were at the same surface weight of 0.05 g, respectively. When the surface is weighed, the rate constant K has the lowest value (0.0115 min^{-1}), and the lowest value of P.D.E is at a surface weight of 0.15 g. The reaction took place for all weights in 75 minutes.

TABLE 4 The (P.D.E.%) and rate constant of RB 4 under UV irradiation vs. catalyst weight of ZnO/CdS nanocomposite at laboratory temperature

Catalyst weight (g)	PDE%														K $(min)^{-1}$
	10 min	15 min	20 min	25 min	30 min	35 min	40 min	45 min	50 min	55 min	60 min	65 min	70 min	75 min	
0.05	2.1	6.03	6.03	10	13.96	20	25.86	25.86	29.31	36.21	38	44.83	46	46.5	0.011
0.075	1.7	2.07	3.922	5.882	9.804	13.730	15.68	21.57	25.49	31.37	35.29	36.74	40.25	41.176	0.0087
0.1	2.05	3.704	5.555	5.555	11.11	14.815	18.52	22.22	24.07	29.63	31.48	35.18	35.18	36.04	0.0073
0.125	1.055	1.818	3.636	5.454	7.273	10.91	14.55	18.18	18.18	23.636	27.27	27.27	30.91	30.91	0.0073
0.15	1.754	1.754	1.786	3.571	5.357	7.143	10.71	12.5	12.5	16.07	16.07	19.64	23.21	23.21	0.005

Effect of pH for RB 4 dye solution

To better understand how the pH function affects how the adsorption interacts with the adsorbent surface and how to employ adsorbents, different media were used. The pH variation in the dye solution has a significant impact on the adsorption capacity during the process [34]. The values (P.D.E%) and the rate constant K are both impacted by the pH of the dye solution, which is a significant influence. After obtaining the best weight of the catalyst surface and the best rate constant, the effect of pH values in the range of 1-11 on the values of P.D.E.% and the rate constant K for the prepared nanoparticle and nanocomposite used in the photocatalytic degradation reaction of the two surfaces (ZnO

and ZnO/CdS) was examined. The concentration of the RB 4 dye solution on each surface that will be exposed to UV light. The photocatalytic effectiveness of the RB 4 dye for each of the two surfaces is displayed in the tables below at various pH levels. The highest P.D.E.% (83.53%) and K value (0.0275 min^{-1}) for the ZnO catalyst nanosurface with RB4 dye solution were found at pH value (7), while the lowest (P.D.E.%) (24.29%) and K value (0.0041 min) were found at pH value (11). According to the Table 5. According to the results for the ZnO surface, the point zero charges PZC of the ZnO surface is pH = 9, and at this pH, the ZnO gains ZnO has a positive charge because of the protons of the functional group. At pH = 7, we see an increase in the values of P.D.E.% and the values of K. In excess of this pH, the ZnO surface is negatively charged [35] and the zero-point charge Finding the point at which the positive charge and negative charge sites on the surface of ZnO are equal requires knowledge of PZC. This can be explained by the fact that ZnO has a neutral surface charge because, at a certain pH level, ZnO has a net zero charge on its surface, which lessens the equal electrical forces acting on its surfaces. This means that if the pH is higher than the pH of P.Z.C., the surface charge is more negative, and if the number is higher, the surface charge is more positive. The pH is lower than P.Z.C pH [36].

TABLE 5 The P.D.E.% and rate constant of RB 4 dye under UV-irradiation vs. different pH for ZnO NPs in laboratory temperature

pH	PDE%														K $(min)^{-1}$
	10 min	15 min	20 min	25 min	30 min	35 min	40 min	45 min	50 min	55 min	60 min	65 min	70 min	75 min	
1	10.6	14.1	15.29	17.65	21.17	24.71	27.06	31.76	35.29	37.65	43.53	49.41	52.94	57.65	0.0193
3	8.23	15.29	18.82	25.88	31.76	35.29	45.88	47.06	55.29	56.47	60.00	62.35	64.71	67.06	0.0117
5	12.5	18.75	31.25	37.5	44.5	51.56	59.38	62.5	65.63	70.31	73.44	78.13	78.13	79.69	0.0189
7	18.82	22.35	36.47	41.18	47.06	52.94	62.35	64.71	67.06	72.94	76.47	81.18	83.53	83.53	0.0275
9	3.53	4.71	4.71	5.88	8.24	11.76	12.94	16.47	20	24.71	25.88	27.06	31.76	35.3	0.0072
11	3.52	3.53	3.53	3.535	6.23	9.26	10.14	13.47	17.22	20.11	21.88	22.1	24.06	24.29	0.0041

The results are presented in Table 6. For the ZnO/CdS nanocomposite surface, the maximum values were for P.D.E.% (53.191%) and K (0.0148 min^{-1}) value at pH = 1 and the lowest value was for P.D.E.% (12.5%) and K (0.0021 min^{-1}) with pH value = 11. The zero-charge point PZC of ZnO/CdS surface is pH = 6, and since the charge of dye RB4 is negative, the acidic medium is the best medium for the photodegradation of the dye (P.D.E.%). This is why for ZnO/CdS surface, the best and highest values of P.D.E.% and K were obtained in a strongly acidic medium (pH = 1).

TABLE 6 The (P.D.E.%) and rate constant of RB 4 dye under UV-irradiation vs. different pH for ZnO/CdS nanocomposite in laboratory temperature

pH	PDE%														K $(min)^{-1}$
	10 min	15 min	20 min	25 min	30 min	35 min	40 min	45 min	50 min	55 min	60 min	65 min	70 min	75 min	
1	4.25	6.38	12.77	19.15	23.4	31.92	36.17	38.29	42.55	44.68	46.81	51.06	53.19	53.2	**0.0148**
3	4.08	8.16	12.25	16.33	20.41	24.49	28.57	30.61	36.74	40.82	44.89	48.98	51.02	51	**0.0136**
5	3.33	4.8	6.62	10.32	14.12	20.22	26.3	26	30	36	38	44	46	48	**0.0118**
7	1.82	3.64	3.64	5.46	7.27	7.27	9.09	10.91	14.5	14.55	14.55	16.36	18.18	18.2	**0.0029**
9	1.75	1.79	3.57	3.57	5.36	7.14	8.93	8.93	10.7	12.5	12.5	16.1	16.1	16.1	**0.0027**
11	1.75	1.78	1.78	1.78	3.57	5.36	5.36	7.14	8.93	10.71	10.71	12.5	12.5	12.5	**0.0021**

Effect of temperature on photo degradation of RB 4 dye

At 25, 30, 35, and 40 °C, the impact of temperature on photodegradation was assessed. According to the first-order kinetic rate constants at different temperatures, the apparent activation energy for the decomposition of RB4 dye was also determined according to Arrhenius equations [37,38].

$$K = A \exp(-Ea/RT) \quad (3\text{-}1)$$

The values of P.D.E.% and k values for each were calculated after research was done on the impact of temperature on the photocatalytic activity of the produced catalysts under the UV illumination for 75 minutes, the P.D.E was raised from 61.403% to 88.612%, and the k was raised from 0.01-0.0141 min^{-1} when the temperature of RB 4 solution was raised. The same result is observed when ZnO/CdS is used, where (P.D.E.) is also increased from 34.214% to 71.929% and k (0.015-0.0166 min^{-1}), in conjunction with raising the temperature of the RB 4 solution. The effect of temperature on the photodegradation of RB 4 dye in the presence of the as-prepared catalysts is probably caused by an increase in the dye frequency and hydroxyl radical molecules colliding at high temperatures, where the photodegradation is maximal and low at lower temperatures, as well as a decrease in the decomposition efficiency of photosynthesis. This is due to the fact that the dye molecule's reaction rate increases with the photocatalyst's surface. Consequently, the absorption increases which facilitates the photodegradation of the colors. All thermal reactions have an activation energy that falls between (7.53975-15.1706367) KJ. Mol^{-1}. The Table 7 provides a summary of the acquired results.

TABLE 7 Photodegradation efficiency (P.D.E.%), the reaction rate constant K, and activation energy Ea of RB4 dye with nanomaterials prepared at different temperatures under the effect of the UV- irradiation

Nanomaterial	T (°C)	P.D.E. % under UV light	K $(min)^{-1}$	Ea (KJ/mol) under UV light
ZnO NPs	25	61.403	0.01	15.1706367
	30	64.912	0.0116	
	35	75.421	0.0124	
	40	88.612	0.0141	
ZnO/CdS	25	34.214	0.0143	7.53975
	30	41.254	0.015	
	35	55.541	0.0156	
	40	71.929	0.0166	

Conclusion

1- The effectiveness of the photocatalytic process technology for treating pollutants, in general, and wastewater, in particular.

2- The use of nanocatalysts in daily life applications because of their broad properties in terms of surface area and small size.

3- Production of nanomaterials by simple chemical methods.

4- The effectiveness of the ZnO catalyst nanosurface compared with the ZnO/CdS nanocatalyst surface in the photodegradation reaction.

5- The effect of the catalysts prepared in the study (ZnO, ZnO /CdS) on the decomposition of dyes, including (Reactive Blue 4) in the presence of ultraviolet radiation.

Acknowledgements

The authors thank College of Science, University of Kufa, for all supports.

Conflict of Interest

The authors declare no conflicts of interest.

Orcid:

Suaad Abd M.A. Noor:
https://orcid.org/0000-0003-4264-2784
Amer M.J. Al-Shamari:
https://orcid.org/0009-0001-1831-3641

References

[1] H. Kazemi Hakki, P. Shekari, A. Najafidoust, N. Dezhvan, M. Seddighi Rad, Influence of calcination temperature and operational parameters on Fe-ZSM-5 catalyst performance in sonocatalytic degradation of phenol from wastewater, *J. Water Environ. Nanotechnol.*, **2021**, *6*, 150–163. [crossref], [Google Scholar], [Publisher]

[2] W. Vallejo, A. Cantillo, B. Salazar, C. Diaz-Uribe, W. Ramos, E. Romero, M. Hurtado, Comparative study of ZnO thin films doped with transition metals (Cu and Co) for methylene blue photodegradation under visible irradiation, *Catalysts*, **2020**, *10*, 528. [crossref], [Google Scholar], [Publisher]

[3] O. Ajani, K. Bello, A. Kogo, Synthesis and characterization of acid dyes based on substituted pyridone using metal complexes (1:2) and study of their application on nylon fabrics (6.6), *Appl. Organomet. Chem.*, **2023**, *3*, 61-72. [crossref], [Google Scholar], [Publisher]

[4] Y. Shen, K. Zhu, D. He, J. Huang, H. He, L. Lei, W. Chen, Tetracycline removal via adsorption and metal-free catalysis with 3D macroscopic N-doped porous carbon nanosheets: nonradical mechanism and degradation pathway, *J. Environ. Sci.*, **2022**, *111*, 351–366. [crossref], [Google Scholar], [Publisher]

[5] A.K. Prajapati, M.K. Mondal, Development of CTAB modified ternary phase α-Fe2O3-Mn2O3-Mn3O4 nanocomposite as innovative super-adsorbent for Congo red dye adsorption, *J. Environ. Chem. Eng.*, **2021**, *9*, 104827. [crossref], [Google Scholar], [Publisher]

[6] P. Praipipat**,** P. Ngamsurach, V. Prasongdee, Comparative reactive blue 4 dye removal by lemon peel bead doping with iron(III) oxide-hydroxide and zinc oxide**,** *ACS omega*, **2022,** *7*, 41744-41758. [crossref], [Google Scholar], [Publisher]

[7] A.A. Nada, M. Nasr, R. Viter, P. Miele, S. Roualdes, M. Bechelany, Mesoporous ZnFe2O4@TiO2 nanofibers prepared by electrospinning coupled to PECVD as highly performing photocatalytic materials, *J. Phys. Chem. C*, **2017**, *121*, 24669–24677. [crossref], [Google Scholar], [Publisher]

[8] H.R. Tantawy, A.A. Nada, A. Baraka, M.A. Elsayed, Novel synthesis of bimetallic Ag–Cu nanocatalysts for rapid oxidative and reductive degradation of anionic and cationic dyes, *Appl. Surf. Sci. Adv.*, **2021**, *3*, 100056. [crossref], [Google Scholar], [Publisher]

[9] H.H. El-Maghrabi, H.R. Ali, S.A. Younis, Construction of a new ternary α-MoO3–WO3/CdS solar nanophotocatalyst towards clean water and hydrogen production from artificial wastewater using optimal design methodology, *RSC advances*, **2017**, *7*, 4409–4442. [crossref], [Google Scholar], [Publisher]

[10] S. Samsami, M. Mohamadi, M.H. Sarrafzadeh, E.R. Rene, M. Firoozbahr, Recent advances in the treatment of dyecontaining wastewater from textile industries: overview and perspectives, *Process Saf. Environ. Prot.*, **2020**, *143*, 138–163. [crossref], [Google Scholar], [Publisher]

[11] A. Balcha, O.P. Yadav, T. Dey, Photocatalytic degradation of methylene blue dye by zinc oxide nanoparticles obtained from precipitation and sol-gel methods, *Environ. Sci. Pollut Res.*, **2016**, *23*, 25485–25493. [crossref], [Google Scholar], [Publisher]

[12] X. Chen, Z. Wu, D. Liu, Z. Gao, Preparation of ZnO photocatalyst for the efficient and rapid photocatalytic degradation of azo dyes, *Nanoscale Res. Lett.*, **2017**, *12*, 1–10. [crossref], [Google Scholar], [Publisher]
[13] A. Fujishima, Z. Xintong, D.A. Tryk, TiO2 photocatalysis and related surface phenomena, *Surf. Sci. Rep.*, **2008**, *63*, 515–582. [crossref], [Google Scholar], [Publisher]
[14] B. Su, M. Zhong, L. Han, M. Wei, Y. Liu, H. Yang, Z. Lei, Eco-friendly preparation of hierarchically selfassembly porous ZnO nanosheets for enhanced photocatalytic performance, *Mater. Res. Bull.*, **2020**, *124*, 110777. [crossref], [Google Scholar], [Publisher]
[15] Z.A. Messaoudi, D. Lahcene, T. Benaissa, M. Messaoudi, B. Z.M. Belhachemi, A. Choukchou-Braham, Adsorption and photocatalytic degradation of crystal violet dye under sunlight irradiation using natural and modified clays by zinc oxide, *Chem. Methodol.*, **2022**, *6*, 661-676. [crossref], [Google Scholar], [Publisher]
[16] R.M. Mhaibes, Z. Arzehgar, M. Mirzaei Heydari, L. Fatolahi, ZnO nanoparticles: A highly efficient and recyclable catalyst for tandem knoevenagel-michael-cyclocondensation reaction, *Asian J. Green Chem.*, **2023**, *7*, 1-8. [crossref], [Google Scholar], [Publisher]
[17] R.J. Kavade, R.G. Khanapure, U.S. Gawali, A.A Patil, S.V. Patil, Degradation of Methyl orange under visible light by ZnO-Polyaniline nanocomposites, *Appl. Organomet. Chem.*, **2022**, 2, 89-100. [crossref], [Pdf], [Publisher]
[18] A.A. Obaid, S.S. Al-ghabban, R. Al-Hussain, Appraising antioxidant and antibacterial activities of zinc oxide nanoparticles synthesized biologically by Iraqi propolis, *Chem. Methodol.*, **2022**, *6*, 366-371. [crossref], [Google Scholar], [Publisher]
[19] M. Farahmandjou, P. Khalili, ZnO nanoparticles synthesized by co-precipitation method; Morphology and optoelectronic study, *Asian J. Green Chem.*, **2021**, *5*, 219-226. [crossref], [Google Scholar], [Publisher].
[20] R. Hajinasiri, M. Esmaeili Jadidi, Synthesis of ZnO nanoparticles via flaxseed aqueous extract, *J. Appl. Organomet. Chem.*, **2022**, *2*, 101-108. [crossref], [Google Scholar], [Publisher]
[21] M.B. Al Taee, B.M. Al Shabander, Study the effect of ZnO concentrations on the photocatalytic activity of TiO_2/cement nanocomposites, *Chem. Methodol.*, **2022**, *6*, 831-841. [crossref], [Google Scholar], [Publisher]
[22] A. Serrà, P. Pip, E. Gómez, L. Philippe, Efficient magnetic hybrid ZnO-based photocatalysts for visiblelight-driven removal of toxic cyanobacteria blooms and cyanotoxins, *Appl. Catal. B: Environ.*, **2020**, *268*, 118745. [crossref], [Google Scholar], [Publisher]
[23] S.N.S. Jefri, A.H. Abdullah, E.N. Muhamad, Response surface methodology: photodegradation of methyl orange by CuO/ZnO under UV light irradiation, *Asian J. Green Chem.*, **2019**, *3*, 271-287. [crossref], [Google Scholar], [Publisher]
[24] A.E. Hashim, F.T. Ibrahim, A Novel Design for Gas Sensor of Zinc Oxide Nanostructure Prepared by Hydrothermal Annealing Technique, *Chem. Methodol.*, **2023**, *7*, 314-324. [crossref], [Pdf], [Publisher]
[25] V.K. Bale, H.R. Katreddi, Synthesis, characterization and catalytic activity of zinc oxide nanoparticles functionalized with metallo-thoiosemicarbazones, *Asian J. Nanosci. Mater.*, **2022**, *5*, 159-173. [crossref], [Pdf], [Publisher]
[26] A. Mari, R. Mookkaiah, M. Elayaperumal, Emblica officinalis leaf extract mediated synthesis of zinc oxide nanoparticles for antibacterial and photocatalytic activities, *Asian J. Green Chem.*, **2019**, *3*, 418-431. [crossref], [Google Scholar], [Publisher]
[27] J. Qiu, M. Li, Y. Wan, S. Zhang, H. Wang, J. Yao, One-pot fabrication of CdxZn1-xS/ZnO nanohybrid using mixed sulfur sources for photocatalysis, *Mater. Res. Bull.*, **2020**, *125*, 110776. [crossref], [Google Scholar], [Publisher]

[28] E. Rezaei-Aghdam, A. Shamel, M. Khodadadi-Moghaddam, G. Ebrahimzadeh Rajaei, S. Mohajeri, Hydrothermal synthesis of ZnO nanoparticles and comparison of its adsorption characteristics with the natural adsorbent (mango peel), *Asian J. Nanosci. Mater.*, **2021**, *4*, 188-200. [crossref], [Google Scholar], [Publisher]

[29] K. Dey, S. Paul, P. Ghosh, Multifunctional additive properties of acrylate based ZnO Nano composite for lubricating oil, *Asian J. Nanosci. Mater.*, **2021**, *4*, 159-170. [crossref], [Google Scholar], [Publisher]

[30] R.J. Kavade; R.G. Khanapure, U.S. Gawali, A.A. Patil, S.V. Patil, Degradation of Methyl orange under visible light by ZnO-Polyaniline nanocomposites, *J. Appl. Organomet. Chem.*, **2022**, *2*, 89-100. [crossref], [Google Scholar], [Publisher]

[31] M. Zirak, O. Moradlou, M.R. Bayati, Y.T. Nien, A.Z. Moshfegh, On the growth and photocatalytic activity of the vertically aligned ZnO nanorods grafted by CdS shells, *Appl. Surf. Sci.*, **2013**, *273*, 391–398. [crossref], [Google Scholar], [Publisher]

[32] S. Khanchandani, S. Kundu, A. Patra, A.K. Ganguli, Shell thickness dependent photocatalytic properties of ZnO/CdS core–shell nanorods, *J. Phys. Chem. C*, **2012**, *116*, 23653–23662. [crossref], [Google Scholar], [Publisher]

[33] F. Aldeek, L. Balan, G. Medjahdi, T. Roques-Carmes, J-P. Malval, C. Mustin, J. Ghanbaja, R. Schneider, Enhanced optical properties of core/shell/shell CdTe/CdS/ZnO quantum dots prepared in aqueous solution, *J. Phys. Chem. C*, **2009**, *113*,– 19458-19467. [crossref], [Google Scholar], [Publisher]

[34] P. Gao, J. Liu, T. Zhang, D.D. Sun, W. Ng, Hierarchical TiO2/CdS "spindle-like" composite with high photodegradation and antibacterial capability under visible light irradiation, *J. Hazard. Mater.*, **2012**, *229–230*, 209–216. [crossref], [Google Scholar], [Publisher]

[35] M. Zirak, O. Akhavan, O. Moradlou, Y.T. Nien, A.Z. Moshfegh, Vertically aligned ZnO@ CdS nanorod heterostructures for visible light photoinactivation of bacteria, J. of Alloys and Compounds, **2014**, *590*, 507–513. [crossref], [Google Scholar], [Publisher]

[36] T.K. Jana, A. Pal, K. Chatterjee, Self assembled flower like CdS–ZnO nanocomposite and its photo catalytic activity, *J. Alloys Compd.*, **2014**, *583*, 510–515. [crossref], [Google Scholar], [Publisher]

[37] H.A.H. Alshamsi, B.S. Hussein, Hydrothermal preparation of silver doping zinc oxide nanoparticles: studys, characterization and photocatalytic activities, *Orient. J. Chem.*, **2018**, *34*, 1898–1907. [Google Scholar], [Publisher]

[38] Y. Zhou, L. Xu, Z. Wu, P. Li, J. He, Optical and photocatalytic properties of nanocrystalline ZnO powders synthesized by a low-temperature hydrothermal method, *Optik*, **2017**, *130*, 673–680. [crossref], [Google Scholar], [Publisher]

[39] R. Raji, K.G. Gopchandran, ZnO nanostructures with tunable visible luminescence; effects of kinetics of chemical reduction and annealing, *J. Sci.: Adv. Mater. Devices*, **2017**, *2*, 51–58. [crossref], [Google Scholar], [Publisher]

[40] H. Selim, A.A. Nada, M. El-Sayed, R.M. Hegazey, R.S. Eglal, M.F. Kotkata, The effect of ZnO and its nanocomposite on the performance of dye-sensitized solar cell, *Nanosci. Nanotechnol.*, **2018**, *12*, 122. [Pdf], [Google Scholar], [Publisher]

[41] K.J. Shanavas, A. Radhakrishnan, B. Beena, Polyaniline/zinc oxide nanocomposite as a remarkable antimicrobial agent in contrast with PANI and ZnO, *Indian J. Adv. Chem. Sci.*, **2018**, *6*, 71-76. [crossref], [Google Scholar], [Publisher]

[42] T.W. Quadri, O. Lukman, O.E. Fayemi, M.M. Solomon, E.E. Ebenso, Zinc oxide nanocomposites of selected polymers; synthesis, characterization and corrosion inhibition studies on mild steel in HCL solution, *ACS Omega*, **2017**, *2*, 8421–8437. [crossref], [Google Scholar], [Publisher]

[43] H. Gholap, A. Gholap, R. Patil, ZnO/CdS Nanocomposite: An Anti-Microbial and Anti-Biofilm Agent, *Adv. Microbiol.*, **2020**, *10*, 166-179. [crossref], [Google Scholar], [Publisher]

[44] B. Bulcha, J.L. Tesfaye, D. Anatol, R. Shanmugam, L.P. Dwarampudi, N. Nagaprasad, V.L. Nirmal Bhargavi, R. Krishnaraj, Synthesis of Zinc Oxide Nanoparticles by Hydrothermal Methods and Spectroscopic Investigation of Ultraviolet Radiation Protective Properties, *J. Nanomater.*, **2021**, *2021*, 8617290. [crossref], [Google Scholar], [Publisher]

[45] P. Basnet, D. Samanta, T.I. Chanu, J. Mukherjee, S. Chatterjee, Assessment of synthesis approaches for tuning the photocatalytic property of ZnO nanoparticles, *SN Applied Sciences*, **2019**, *1*, 633. [crossref], [Google Scholar], [Publisher]

[46] M. Alsawalha, Catalytic Activity and Kinetic Modeling of Various 173 Modules HZMS-5 and Treated MCM-41 Catalysts, for the Liquid-Phase Ketalization of Glycerol with Acetone, *Front. Chem.*, **2019**, *7*, 799. [crossref], [Google Scholar], [Publisher]

[47] A.M. Mostafa, E.A. Mwafy, Synthesis of ZnO and Au @ ZnO core / shell nano-catalysts by pulsed laser ablation in different, *J. Mater. Res. Technol.*, **2020**, *9*, 3241-3248. [crossref], [Google Scholar], [Publisher]

[48] Z. Zhang, B. Jiang, F. He, Z. Fu, J. Xu, Comparative Study on Kinetics of Ethylene and Propylene Polymerizations with Supported Ziegler – Natta Catalyst: Catalyst Fragmentation Promoted by Polymer Crystalline Lamellae, *Polymers (Basel)*, **2019**, *11*, 358. [crossref], [Google Scholar], [Publisher]

[49] T. Virtanen, G. Rudolph, A. Lopatina, B. Al-rudainy, Analysis of membrane fouling by Brunauer-Emmet-Teller nitrogen adsorption/ desorption technique, *Scientific reports*, **2020**, *10*, 1–10. [crossref], [Google Scholar], [Publisher]

[50] M. Pirsaheb, H. Hossaini, S. Nasseri, N. Azizi, B. Shahmoradi, T. Khosravi, Optimization of photocatalytic degradation of methyl orange using immobilized Scoria-Ni/TiO2 nanoparticles, *J. Nanostructure Chem.*, **2020**, *10*, 143–159. [crossref], [Google Scholar], [Publisher]

[51] R.D.C. Soltani, M. Mashayekhi, M. Naderi, G. Boczkaj, S. Jorfi, M. Safari, Sonocatalytic degradation of tetracycline antibiotic using zinc oxide nanostructures loaded on nano-cellulose from waste straw as nanosonocatalyst, *Ultrason. Sonochem.*, **2019**, *55*, 117–124. [crossref], [Google Scholar], [Publisher]

[52] A.K. Chauhan, N. Kataria, V.K. Garg, Green fabrication of ZnO nanoparticles using Eucalyptus spp. leaves extract and their application in wastewater remediation, *Chemosphere*, **2020**, *247*, 125803. [crossref], [Google Scholar], [Publisher]

[53] C.S. Santana, M.D.N. Ramos, C.C.V. Velloso, A. Aguiar, Kinetic evaluation of dye decolorization by fenton processes in the presence of 3-hydroxyanthranilic acid, *Int. J. Environ. Res. Public Health*, **2019**, *16*, 1602. [crossref], [Google Scholar], [Publisher]

[54] N.A. Patil, D.R. Shinde, P.D. Patil, Green Synthesis of Gold Nanoparticles Using Extract of Ginger, Neem, Apta, Umber Plants and Their Characterization Using XRD, UV-Vis Spectrophotometer, *J. Appl. Organomet. Chem.*, **2023**, *3*, 1-12. [crossref], [Pdf], [Publisher]

[55] M. Dhange, S. Patwari, N. Kaminwar, B.R. Madje, D.P. Rajani, R.U. Pokalwar, Antituberculosis activity, Ssynthesis of 3-((1H-benzo[d]imidazol-2-ylthio)methyl)-2-chloroquinoline derivatives using copper nanoparticles grafted on carbon microspheres, *J. Appl. Organomet. Chem.*, **2023**, *3*, 39-51. [crossref], [Pdf], [Publisher]

[56] O. Ajani, K. Bello, A. Kogo, Synthesis and Characterization of Acid Dyes Based on Substituted Pyridone Using Metal Complexes (1:2) and Study of their Application on Nylon Fabrics (6.6), *J. Appl. Organomet. Chem.*, **2023**, *3*, 61-72. [crossref], [Google Scholar], [Publisher]

[57] V. Safari Fard, Y. Davoudabadi Farahani, An amine/imine functionalized microporous MOF as a new fluorescent probe exhibiting selective sensing of Fe_3+ and Al_3+ over mixed metal ions, *J. Appl. Organomet. Chem.*, **2022**, *2*, 165-179. [crossref], [Google Scholar], [Publisher]
[58] H. Shayegan, V. Safari Fard, H. Taherkhani, M.A. Rezvani, Efficient Removal of Cobalt(II) Ion from Aqueous Solution Using Amide-Functionalized Metal-Organic Framework, *J. Appl. Organomet. Chem.*, **2022**, *2*, 109-118. [crossref], [Google Scholar], [Publisher]

How to cite this article: Suaad Abd M.A. Noor, Amer M.J. Al-Shamari. High photocatalytic performance of ZnO and ZnO/CdS nanostructures against reactive blue 4 dye. *Eurasian Chemical Communications*, 2023, 5(9), 776-793. **Link:** https://www.echemcom.com/article_171849.html